

# CDDT: Fast Approximate 2D Ray Casting for Accelerated Localization

Corey H. Walsh<sup>1</sup> and Sertac Karaman<sup>2</sup>

**Abstract**—Localization is an essential component for autonomous robots. A well-established localization approach combines ray casting with a particle filter, leading to a computationally expensive algorithm that is difficult to run on resource-constrained mobile robots. We present a novel data structure called the Compressed Directional Distance Transform for accelerating ray casting in two dimensional occupancy grid maps. Our approach has near constant time ray casting performance for a fixed size map, in contrast with other methods which display long tail query time distributions. Our experimental results show that the proposed algorithm approximates the performance characteristics of reading from a three dimensional lookup table of ray cast solutions while requiring two orders of magnitude less memory and precomputation. This results in a particle filter algorithm which can maintain 2500 particles with 61 ray casts per particle at 40Hz, using only a single CPU thread onboard a mobile robot.

## I. INTRODUCTION

Determining a robot's location and orientation in a known environment, also known as localization, is an important and challenging problem in the field of robotics. Particle filters are a popular class of Monte Carlo algorithms used to track the pose of mobile robots by iteratively refining a set of pose hypotheses called particles. After determining an initial set of particles, the particle filter updates the position and orientation of each particle by applying a movement model based on available odometry data. Next, the belief in each particle is updated by comparing sensor readings to a map of the environment. Finally, the particles are resampled according to the belief distribution and algorithm repeats.

While particle filters provide a robust and general framework for solving the localization problem, they can be computationally expensive due to both the number of particles which must be maintained and the evaluation of the sensor model. In robots with range sensors such as LiDAR or Sonar, ray casting is frequently used to compare sensor readings with the ground truth distance between the hypothesis pose and obstacles in a map. Ray casting itself is a complex operation, and a single evaluation of the sensor model may require tens of ray casts. Many effective particle filters maintain thousands of particles, updating each particle tens of times per second. As a result, millions of ray cast operations may be resolved per second, posing a significant computational challenge for resource constrained systems.

<sup>1</sup>Corey H. Walsh is with the Department of Computer Science and Engineering, Massachusetts Institute of Technology, Cambridge, MA 02139, USA [chwalsh@mit.edu](mailto:chwalsh@mit.edu)

<sup>2</sup>Sertac Karaman is with the Laboratory for Information and Decision Systems, Massachusetts Institute of Technology, Cambridge, MA 02139, USA [sertac@mit.edu](mailto:sertac@mit.edu)

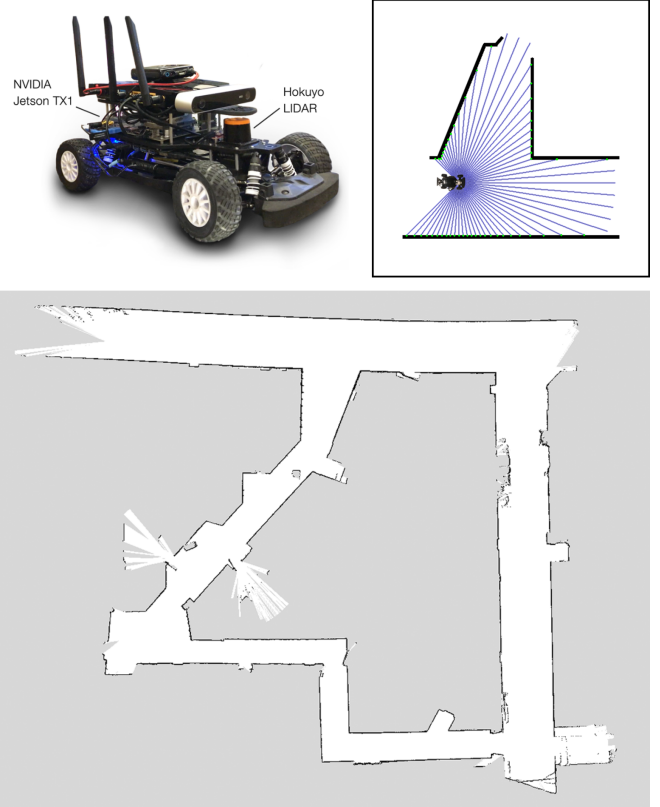


Fig. 1. Robotic RACECAR mobile platform (top left). Synthetic occupancy grid map with the 61 ray cast beams used in the particle filter sensor model visualized in blue (top left). Stata basement occupancy grid map (bottom).

Several well known algorithms exist for ray casting in two dimensional spaces such as Bresenham's Line algorithm [1] and ray marching [2]. Both algorithms work by iteratively checking points in the map starting at the query point and moving in the ray direction until an obstacle is discovered. This process does not provide constant performance because the number of memory reads depends on the distance to the nearest obstacle.

To combat the computational challenges of ray casting while localizing in a two-dimensional map, Fox et al. [3] suggest the use of a large three-dimensional lookup table (LUT) to store expected ranges for each discrete  $(x, y, \theta)$  state. While this is simple to implement and does result in large speed improvements as compared to ray casting, it can be prohibitively memory intensive for large maps and/or resource constrained systems. In a 2000 by 2000 occupancy map, storing ranges for 200 discrete directions would require over 1.5GB. While this memory requirement may be acceptable in many cases, it scales with the square

of map size - a 4000 by 4000 map would require over 6GB for the same angular discretization, which is larger than the random-access memory on-board many mobile robots.

The main contribution of this paper is a new acceleration data structure, called the Compressed Directional Distance Transform (CDDT) which allows near constant time two dimensional ray casting queries for a fixed map. The algorithm is benchmarked against several commonly used ray casting methods. We provide an open-source implementation of CDDT and the other methods evaluated here in a library called RangeLibc<sup>3</sup>. The CDDT algorithm has been applied to a particle filter localization algorithm<sup>4</sup>, allowing 2500 particles to be maintained at 40Hz with 61 ray casts per particle on a NVIDIA Jetson TX1 embedded computer.

We observe two orders of magnitude improvement in memory consumption when compared to the lookup table method, with little sacrifice in computation time. Additionally, we observe a large speedup when compared to the other ray casting methods considered, with similar memory requirements.

While we have not yet implemented CDDT with graphics processing hardware, one motivation of our approach is that the data structure would easily fit into GPU memory, even for large maps. We also recognize the potential for our method to allow on-line updates to the map without requiring a full re-computation of the acceleration structure, which is useful when the environment is not fully known at startup.

The paper is organized as follows. Section 2 discusses existing two dimensional ray casting methods. Section 3 introduces terminology used throughout the paper. Section 4 describes the new algorithm and its various optimizations. Section 5 gives a theoretical analysis of CDDT's asymptotic complexity. Section 6 describes our experimental results and comparisons. Finally, section 7 presents our conclusions.

## II. RELATED WORK

Bresenham's line algorithm [1] is one of the most widely used methods for two dimensional ray casting in occupancy grids. The algorithm incrementally determines the set of pixels that approximate the trajectory of a query ray starting from the query point  $(x, y)_{query}$  and progressing in the  $\theta_{query}$  direction one pixel at a time. The algorithm terminates once the nearest occupied pixel is discovered, and the euclidean distance between that occupied pixel and  $(x, y)_{query}$  is reported. This algorithm is widely implemented in particle filters due to its simplicity and ability to operate on a dynamic map. The primary disadvantage is that it is slow, potentially requiring hundreds of memory accesses for a single ray cast. While average performance is highly environment dependent, Bresenham's Line algorithm is linear in map size in the worst case.

Similar to Bresenham's Line, the ray marching [2] algorithm checks points along the line radiating outwards from the query point until an obstacle is encountered. The

primary difference is that ray marching makes larger steps along the query ray, thereby avoiding unnecessary memory reads. Beginning at  $(x, y)_{query}$ , the ray marching algorithm proceeds in the  $\theta_{query}$  direction, stepping along the line by the minimum distance between each visited point and the nearest obstacle in any direction. The algorithm terminates when the query point coincides with an obstacle in the map. A precomputed euclidean distance transform of the occupancy map provides the distance between visited points and the nearest obstacles.

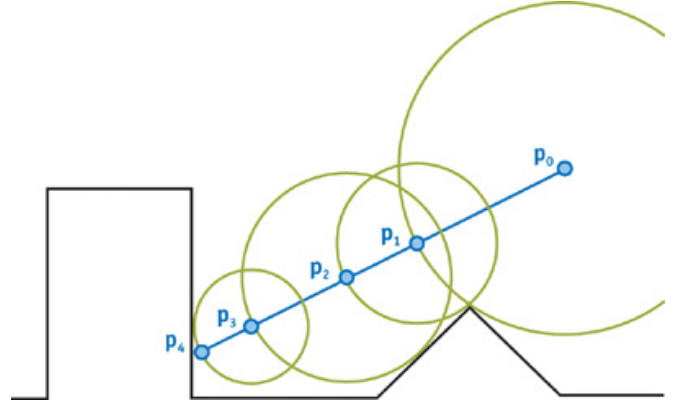


Fig. 2. Visualization of ray marching starting at  $p_0$  towards  $p_4$ . Green circle around each query point represents the distance to the nearest obstacle from that point. Blue dots represent the query points, labeled in order of execution. From [4].

Ray marching is on average much faster than Bresenham's line, but edge cases exist in which the theoretically asymptotic runtime is equivalent. As noted by Zuiderveld et al. [5], the traversal speed of rays rapidly decreases as sampled positions approach obstacles. For this reason, rays which travel parallel to walls progress very slowly as compared to those passing through open areas. Thus, the performance of ray marching exhibits a long tail distribution as seen in (Fig. 10) which negatively impacts average runtime as compared to the median, which can be problematic for near real time algorithms.

As previously described, a common acceleration technique for two dimensional ray casting is to precompute the ray distances for every state in a discrete grid and store the results in a three dimensional LUT for later reference. Any ray casting technique may be used to compute the table. In the authors' implementation ray marching is used for its fast performance compared to Bresenham's Line and its high accuracy. Theoretically, the LUT approach has constant query runtime, though actual performance access pattern dependent as CPU caching effects are significant in practice.

State space discretization implies approximate results, since intermediate states must be rounded onto the discrete grid. While the effect of rounding query position is small, rounding  $\theta_{query}$  may have significant effects since angular roundoff error accumulates with ray length. For queries  $(x, y, \theta)_{query}$  discretized into  $\lfloor (x, y, \theta) \rfloor$ , the distance between the end of the ray  $\lfloor (x, y, \theta) \rfloor$  and its projection onto the

<sup>3</sup>[https://github.com/kctess5/range\\_libc](https://github.com/kctess5/range_libc)

<sup>4</sup>[https://github.com/mit-racecar/particle\\_filter](https://github.com/mit-racecar/particle_filter)

line implied by  $(x, y, \theta)_{query}$  becomes large as the length of the ray increases. Although the error induced by discretization may be unacceptable for computer graphics applications, it is generally acceptable for probabilistic algorithms such as the particle filter since error is anticipated and directly modeled.

More generally, due to varied handling of edge cases and ambiguities in the problem of determining distance between any point and the nearest obstacle in a particular direction, most 2D ray casting algorithms do not provide exactly consistent results for every query. However, on average error between results from each of the methods discussed is small. Any error that does exist is dominated by error inherent in distance sensors.

Rather than simply rounding to the nearest grid state, one may improve accuracy of queries which lie between discrete states by querying the neighboring states and interpolating the results. Interpolation requires greater than one memory read and a small amount of arithmetic, and is therefore slower on average than rounding to the nearest grid state. Since we are evaluating the performance of these methods in the context of particle filter localization, the number of particles maintained is more important than ray cast accuracy so we do not perform interpolation.

### III. PROBLEM FORMULATION AND NOTATION

We define the problem of ray casting in occupancy grids as follows. We assume a known occupancy grid map in which occupied cells have value 1, and unoccupied cells have value 0. Given a query pose  $(x, y, \theta)_{query}$  in map space, the ray cast operation finds the nearest occupied pixel  $(x, y)_{collide}$  which lies on the ray starting at the position  $(x, y)_{query}$  pointing in the  $\theta_{query}$  direction, and returns the euclidean distance  $d_{ray}$  between  $(x, y)_{query}$  and  $(x, y)_{collide}$ .

$$d_{ray} = \left\| \begin{pmatrix} x \\ y \end{pmatrix}_{query} - \begin{pmatrix} x \\ y \end{pmatrix}_{collide} \right\|_2$$

We refer to  $(x, y, \theta)_{query}$  as the query pose, and  $(x, y)_{query}$  as the query point. We denote the discretized query pose as  $\lfloor (x, y, \theta)_{query} \rfloor$ . A  $\theta$  slice through the LUT refers to all table entries for that particular  $\lfloor \theta \rfloor$ . The number of discrete  $\lfloor \theta \rfloor$  values is denoted  $\theta_{discretization}$ . Fig. 3 demonstrates our chosen coordinate system.

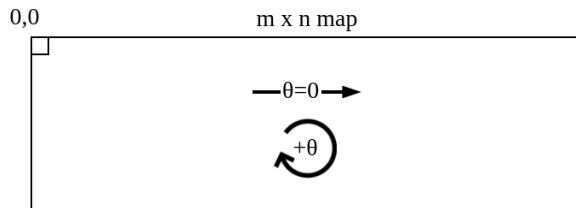


Fig. 3. Occupancy grid map coordinate system

### IV. THE COMPRESSED DIRECTIONAL DISTANCE TRANSFORM ALGORITHM

Although the three dimensional table used to store precomputed ray cast solutions in a discrete state space is inherently large, it is highly compressible. This is most apparent in the cardinal directions, in which adjacent values along a particular dimension of the table increase by exactly one unit of distance for unobstructed positions as in Fig. 4. Our data structure is designed to compress this redundancy while still allowing for fast queries in near constant time. We accomplish this though through what we refer to as a Compressed Directional Distance Transform described here.

				3	2	1	0
				1	0	-	-
				2	1	0	-
				3	2	1	0

Fig. 4. Occupancy grid (left) and associated LUT slice for  $\theta = 0$  (right).

The euclidean distance transform of an occupancy grid map stores the distance to the nearest obstacle in any direction  $\theta$  for each possible  $\lfloor (x, y) \rfloor$  in the map. In contrast, what we call a directional distance transform (DDT) stores the distance to the nearest obstacle in a particular direction  $\lfloor \theta \rfloor$  for every  $\lfloor (x, y) \rfloor$ . The key difference between a single  $\theta$  slice of the LUT and a directional distance transform for the same  $\theta$  is the way in which it is computed and indexed. To compute the LUT slice, ray casting is performed in the  $\theta$  direction for every  $\lfloor (x, y) \rfloor$ . At runtime, each  $(x, y)_{query}$  is discretized to  $\lfloor (x, y)_{query} \rfloor$  and the LUT slice is directly indexed.

In contrast, to compute the DDT, the obstacles in the map are rotated about the origin by  $-\lfloor \theta \rfloor$  and ray casting is implicitly performed in the  $\theta = 0$  direction, as demonstrated by Fig. 5. Then, to index the table for a query  $(x, y, \theta)_{query}$ , one discretizes to  $\lfloor (x, y, \theta)_{query} \rfloor$ , rotates  $\lfloor (x, y)_{query} \rfloor$  about the origin, and uses the rotated coordinates  $\lfloor (x, y, \theta)_{query} \rfloor_{rot}$  to (implicitly) index into the DDT. Thus, roughly the same operation is computed in both the DDT and the LUT, but while one changes the ray cast direction to populate the LUT, one rotates scene geometry and ray casts in a constant direction to populate the DDT.

We define  $P_{DDT_\theta}$  as the three by three transformation matrix which projects vectors into the coordinate space of the DDT in the  $\theta$  direction. While it is true that the transformation of the scene geometry introduces small errors as compared to ray casting for each cell, as previously discussed, small errors do not significantly impact particle filter localization performance.

The distinction between the LUT slice and the DDT may be subtle, but it has an important effect. Since ray casting is always performed in the  $\theta = 0$  direction to populate the DDT, all values in the same row of the DDT either increase by one unit with respect to their neighbor in the  $\theta = 0$

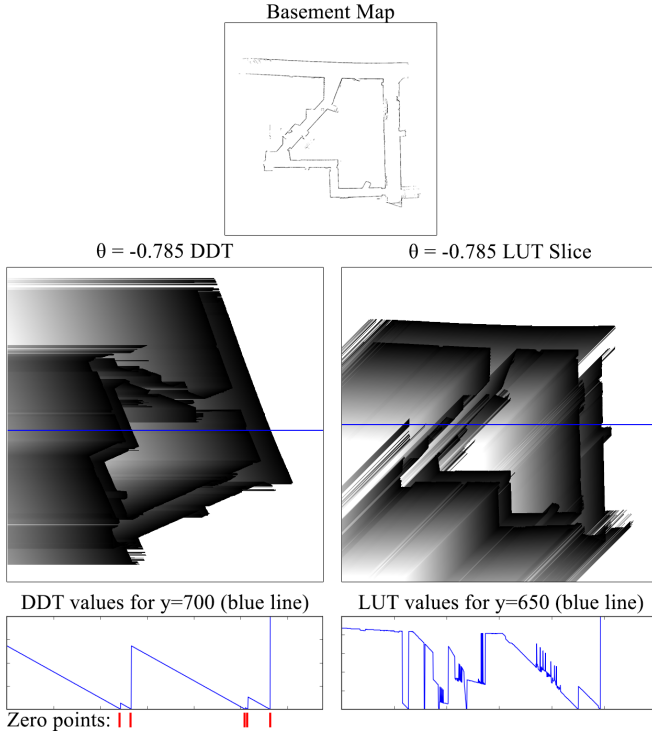
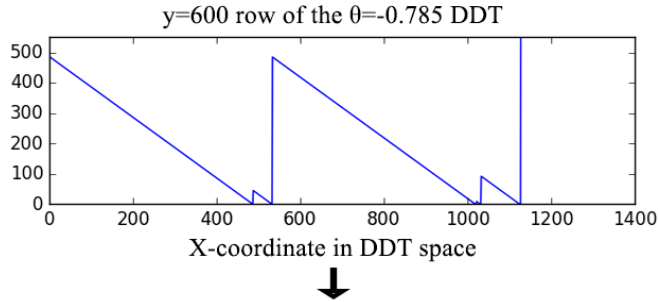


Fig. 5. Comparison between a DDT and a LUT slice for the same value of theta. Each row in the DDT is characterized by a sawtooth function.

direction or go to zero. Thus each row of the DDT may be characterized as a sawtooth function where the zero points correspond to obstacles in the map. This characterization as a sawtooth function provides a natural method of lossless compression: keep the zero points and discard the rest.



Zero points: {486 532 1018 1020 1030 1031 1124 1125 1126}

Fig. 6. Demonstration of compression from a sawtooth function to a list of zero points. Consecutively valued zero points exist projected scene geometry spans greater than one unit along the x axis.

The conversion from DDT to CDDT slice is done by storing the  $x$  coordinates of each zero point for every row of the DDT as demonstrated for a single row in Fig. 6. At query time, the sawtooth function (i.e. exactly the distance to the nearest obstacle in the query direction) encoded in the DDT may be quickly recovered by performing binary search for nearest zero point in the correct row of the CDDT slice. We refer to the list of zero points for a single row as a CDDT bin. Similar to the LUT, the full CDDT is defined as every

CDDT slice for all discrete values of  $\theta$ .

For performance, it is not necessary to compute or store the full DDT, but rather the CDDT may be directly constructed by projecting each obstacle into the coordinate space of the DDT for every  $[\theta]$  and storing its projected  $x$  coordinate in the CDDT bin corresponding to its  $y$  coordinate and  $[\theta]$ . After all geometry has been projected into the CDDT, each bin is sorted to facilitate later indexing. Not only does the direct construction of the CDDT greatly reduce the amount of memory required to store a lookup table, it also reduces data structure precomputation time since ray casting every discrete state is not necessary.

While conceptually simple, implementing the CDDT data structure construction and traversal routines requires careful consideration in order to capture all edge cases and to minimize unnecessary computation. In this sense, it is more complex to implement than the alternatives considered, however there are many opportunities for optimization which yield real-world speed up. To ease this burden, we provide our implementation<sup>3</sup> as well as Python wrappers under the Apache 2.0 license.

#### A. CDDT Construction Algorithm

---

```

edge_map ← map − morphological_erosion(map)
Initialize  $\theta_{discretization}$  empty CDDT slices
for  $\theta \in \{[\theta]\}$  do
  for each occupied pixel  $(x, y) \in edge\_map$  do
     $(x, y)_{DDT_\theta} = P_{DDT_\theta} * \begin{pmatrix} x \\ y \\ 1 \end{pmatrix}$ 
    for each CDDT bin overlapping with  $y_{DDT_\theta}$  do
      bin.append( $x_{DDT_\theta}$ )
    end for
  end for
  for each CDDT bin do
    bin = sort(bin)
  end for
end for

```

---

#### B. CDDT Query Algorithm

---

```

function ray_cast( $(x, y, \theta)_q$ )
   $(x, y)_{DDT_{\theta_q}} = P_{DDT_{\theta_q}} * \begin{pmatrix} x_q \\ y_q \\ 1 \end{pmatrix}$ 
  bin ← zero points in row  $y_{DDT_{\theta_q}}$  of CDDT slice  $\theta_q$ 
   $x_{collide} = \text{smallest element } x_{collide} > x_{DDT_{\theta_q}} \in \text{bin}$ 
  return abs( $x_{DDT_{\theta_q}} - x_{collide}$ )
end function

```

---

In our implementation we switch between linear and binary search to find  $x_{collide}$  in a given CDDT bin depending on the number of zero points in that bin. While binary search is theoretically optimal for sorted arrays, in practice linear search has a superior memory access pattern and is therefore faster in small searches.

### C. Further Optimizations

A side effect of extracting zero points from each row of the DDT is the introduction of rotational symmetry. Not only can a row of the DDT in the  $\theta$  direction be reconstructed from the zero points, but also a row of the DDT in the  $\theta + \pi$  direction as in Fig. 7. Therefore, one only need compute and store CDDT slices for  $0 \leq [\theta] < \pi$  and the DDT for  $0 \leq [\theta] < 2\pi$  may be inferred by reversing the search direction, resulting in a factor of two reduction in memory usage.

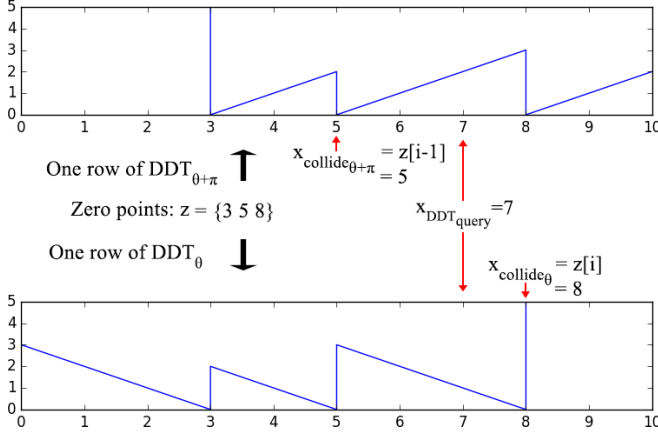


Fig. 7. Demonstration of reconstructing rows of two DDT slices from a single set of zero points.

In addition to the aforementioned reduction in memory usage, rotational symmetry may be exploited in scenarios where ray casts are performed radially around a single point. While traversing the data structure to resolve a ray cast query  $(x, y, \theta)$ , the ray cast for  $(x, y, \theta + \pi)$  may be resolved with a single additional memory read. Once a search algorithm is used to discover the index  $i$  of  $x_{collide_{\theta}}$  in the CDDT, the index of  $x_{collide_{\theta+\pi}}$  is simply  $i - 1$  as in Fig. 7. For example, this symmetry can be used in robots with laser scanners sweeping angles larger than  $180^\circ$  to reduce the number of data structure traversals required to compute the sensor model by up to a factor of two.

With small modifications, another factor of two reduction in CDDT size could be attained by storing zero points as 16 bit integers rather than 32 bit floats with little precision loss.

While the authors did not implement the necessary changes, we conjecture that the CDDT algorithm could be modified to allow incremental updates to the map. In both ray marching and the LUT approach, any change in the map introduces inconsistencies to the acceleration data structure requiring a full re-initialization. As demonstrated by our experiments, initializing the three dimensional LUT is a highly computational process. Similarly, computing a euclidean distance transform for ray marching can be expensive. Therefore neither ray marching nor the LUT can be easily used with dynamic maps such as in SLAM algorithms. Despite being the slowest option evaluated, Bresenham's Line algorithm is one of the most commonly used techniques since it operates directly on the grid map without an acceleration data structure.

To allow incremental update of the CDDT, the sorted vector data structure used in our implementation to store zero points should be replaced with an alternative which allows for  $O(\log n)$  insertion and deletion, such as a randomized skip list. To aid in zero point deletion, pointers could be maintained correlating each cell in the occupancy grid with its associated zero points for each CDDT slice with a constant factor increase in memory usage. In this case, the cost of toggling the state of a cell in the occupancy grid would be  $O(\theta_{discretization} \log n)$  where  $n$  is the number of elements in each associated CDDT bin. For most occupancy grid maps of real environments, the value of  $n$  is small, and in any case is bounded by the size of the map, so  $\log n$  is bounded by a small constant factor. Therefore, the cost of update with becomes  $O(\theta_{discretization})$  which is likely not prohibitive for real-time performance in dynamic maps.

Skip list traversal is likely to be less efficient than binary search on sorted vectors due to worse cache characteristics. However, the authors expect it to still be faster than performing Bresenham's Line algorithm, and therefore recommend that this modification be the subject of future research.

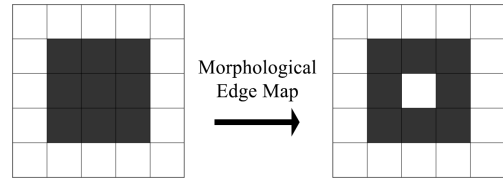


Fig. 8. Example map left, morphological edge map right.

By removing entries in the CDDT which can never possibly result in a ray collision, it is possible to further reduce the memory footprint of the data structure. Consider a 3x3 block of obstacles in an otherwise empty map as in Fig. 8. The center obstacle will never be the nearest neighbor in any ray casting query, because any such query would first intersect with one of the 8 surrounding obstacles. To exploit this, one can take the morphological edge map of the occupancy grid prior to CDDT generation without loss of generality. During ray casting on the CDDT data structure, we check the occupancy grid to ensure that the query point itself is not an obstacle and return a distance of zero if so in order to prevent incorrect results when ray casting from the middle of obstacles removed during the morphological operation. In dense maps, this results in a significant reduction in both memory usage and construction time.

Additionally, consider a line of obstacles aligned along the X-axis. Every element in this line will be projected into a single zero point bin in the  $\theta = 0$  CDDT slice. However, the middle elements of the line will never result in a collision. Any ray cast from points on the line of obstacles will return early in the occupancy grid check, and any ray cast from non-overlapping points co-linear in the  $\theta$  or  $\theta + \pi$  directions will intersect either the first or last obstacle in the line. Therefore in the  $\theta = 0$  CDDT slice, one may discard the zero points corresponding to the middle elements without introducing error. This form of optimization is simple to compute in



the cardinal directions, but non-trivial for arbitrary  $[\theta]$  not aligned with an axis. Rather than analytically determining which obstacles may be discarded, it is simpler to prune the data structure by ray casting from every possible state, discarding any unused zero point.

Pruning does increase pre-computation time, rendering it incompatible with incremental update. However, the reduction of memory usage is worthwhile for static maps. In addition to memory reduction, we find that pruning slightly improves runtime performance, likely as a result of improved caching characteristics and the reduced number of zero points. We refer to the pruned datastructure as PCDDT.

## V. ANALYSIS

In this section, we refer to the width and height of the source occupancy grid map as  $w$  and  $h$ , respectively. We refer to the diagonal length across the map as  $d_{w,h} = \sqrt{w^2 + h^2}$ . The CDDT algorithm requires the original map data to check for overlaps between  $(x, y)_{query}$  and obstacles prior to searching CDDT bins. Additionally, for each occupied map pixel, a total of  $\theta_{discretization}$  float values are stored in the CDDT bins. Thus, the memory usage of the CDDT data structure is  $O(n * \theta_{discretization} + w * h)$  where  $n$  is the number of occupied pixels in the edge map. Since we must sort each bin after CDDT construction, pre-computation time is at worst  $O(n * \theta_{discretization} + d_{w,h}^2 * \theta_{discretization} * \log(d_{w,h}))$  for the same definition of  $n$ . In practice it is closer to  $n * \theta_{discretization} + d_{w,h} * \theta_{discretization}$  since each CDDT bin has a small number of elements on average, as evidenced by the high demonstrated compression ratio.

The pruning operation described in IV-C reduces memory requirement, with a computational cost of  $O(w * h * \theta_{discretization} * O(\text{calc.range})_{CDDT})$ . The precise impact of pruning is scene dependent and difficult to analyze in the general case.

The ray cast procedure has three general steps: projection into CDDT coordinate space, the search for nearby zero points, and the computation of distance given the nearest zero point. The first and last steps are simple arithmetic, and therefore are theoretically constant time. The second step involves searching for a value in a sorted array of zero points. As previously discussed in IV-C, the number of zero points in each CDDT bin tends to be small and is bounded in map size. Thus, at worst the search operation requires  $\log(d_{w,h})$  which is a small constant value for a fixed size map. Therefore, for a given map, our algorithm provides  $O(1)$  query performance.

## VI. EXPERIMENTS

We have implemented the proposed algorithm in the C++ programming language, as well as Bresenham’s Line, ray marching, and the LUT approach for comparison. Our source code<sup>1</sup> is available for use and analysis, and Python wrappers are also provided for easier usage. All synthetic benchmarks were performed on a desktop computer on a Intel Core i5-4590 CPU @ 3.30GHz with 16GB DDR3 ram @ 1333MHz, running Ubuntu 14.04.

Basement Map, $\theta_{discretization}$ : 108		
Method	Memory Usage	Init. Time
Bresenham’s Line	1.37 MB	0.006 sec
Ray Marching	5.49 MB	0.16 sec
CDDT	6.34 MB	0.067 sec
PCDDT	4.07 MB	2.2 sec
Lookup Table	296.63 MB	15.3 sec

Synthetic Map, $\theta_{discretization}$ : 108		
Method	Memory Usage	Init. Time
Bresenham’s Line	1 MB	0.004 sec
Ray Marching	4 MB	0.13 sec
CDDT	2.71 MB	0.03 sec
PCDDT	1.66 MB	0.74 sec
Lookup Table	216 MB	9.1 sec

Fig. 9. Construction time and memory footprint of each method. Ranges stored in lookup table with 16 bit integers, initialized with ray marching.

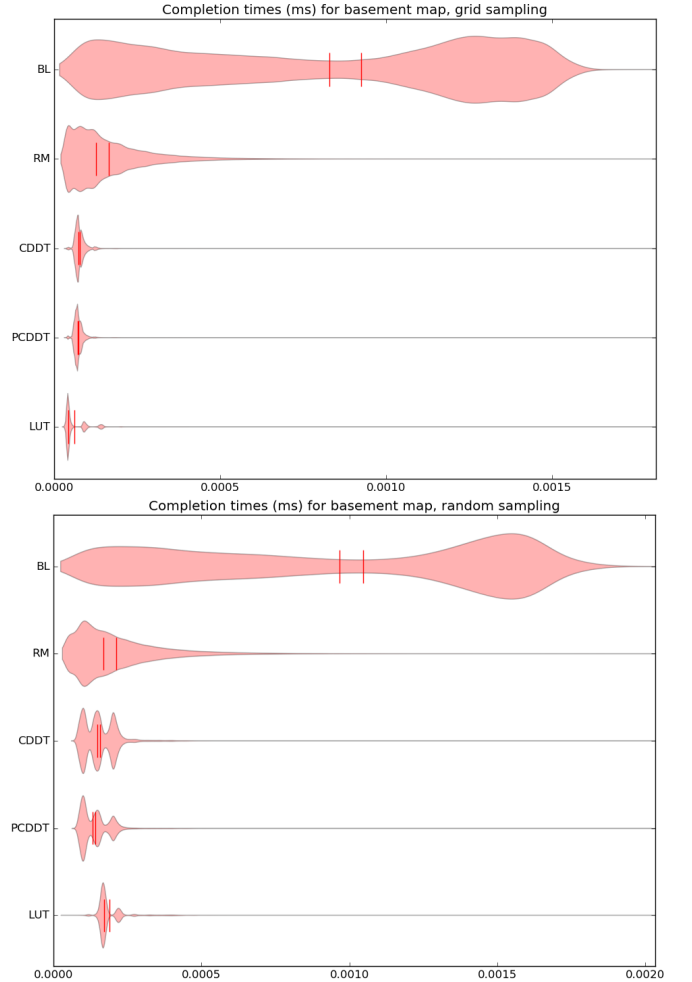


Fig. 10. Violin plots demonstrating histogram of completion time over a large number of queries for each ray cast method. Basement map. X axis shows time in milliseconds, and Y axis shows the number of queries that completed after that amount of time.

We evaluate algorithm performance in two synthetic benchmarks, using two different maps. The first “random”

benchmark computes a ray cast for each point in a uniformly spaced grid over the three dimensional state space. The second "grid" benchmark performs a large number of ray casts for randomly generated states. The so called Synthetic map (Fig. 1) was created with Adobe Photoshop, whereas the basement map (Fig. 6) was created via a SLAM algorithm on the RACECAR platform<sup>5</sup> while navigating the Stata basement loop.

Synthetic Map Ray Cast Benchmarks				
Random Sampling				
Method	Mean	Median	IQR	Speedup
BL	1.19e-06	1.41e-06	7.71e-07	1
RM	1.52e-07	1.25e-07	1.05e-07	7.81
CDDT	1.24e-07	1.05e-07	5.3e-08	9.59
PCDDT	1.19e-07	1.01e-07	5e-08	10.02
LUT	1.82e-07	1.68e-07	1.4e-08	6.55
Grid Sampling				
Method	Mean	Median	IQR	Speedup
BL	1.03e-06	1.20e-06	6.79e-07	1
RM	1.27e-07	1.03e-07	1.06e-07	8.06
CDDT	7.02e-08	6.8e-08	1e-08	14.63
PCDDT	6.94e-08	6.8e-08	9e-09	14.80
LUT	6.33e-08	4.2e-08	4.6e-08	16.21

Basement Map Ray Cast Benchmarks				
Method	Mean	Median	IQR	Speedup
Random Sampling				
BL	9.66e-07	1.05e-06	1.08e-06	1
RM	2.12e-07	1.68e-07	1.64e-07	4.56
CDDT	1.58e-07	1.49e-07	9.1e-08	6.13
PCDDT	1.41e-07	1.32e-07	6.5e-08	6.83
LUT	1.89e-07	1.7e-07	2.1e-08	5.10
Grid Sampling				
Method	Mean	Median	IQR	Speedup
BL	8.29e-07	9.24e-07	9.53e-07	1
RM	1.65e-07	1.26e-07	1.34e-07	5.02
CDDT	7.69e-08	7.2e-08	1.6e-08	10.78
PCDDT	7.32e-08	7e-08	1.4e-08	11.33
LUT	6.13e-08	4.3e-08	4.6e-08	13.53

Fig. 11. Synthetic benchmark ray cast query runtime statistics for the Synthetic map (top) and Basement map (bottom). All times listed in seconds, speedup relative to Bresenham's Line

To demonstrate real world performance, we have implemented<sup>4</sup> the particle filter localization algorithm using a beam mode sensor model. We provide information about the ray cast performance of each algorithm while being used to compute the sensor model (Fig. 13), and the maximum number of particles each method was able to support in real time (Fig. 14). In all particle filter benchmarks, we use the NVIDIA Jetson TX1 embedded computer onboard the RACECAR platform. We use a single thread for computing the Monte Carlo update step, though it could be easily parallelized across multiple threads for additional performance.

<sup>5</sup><http://racecar.mit.edu>

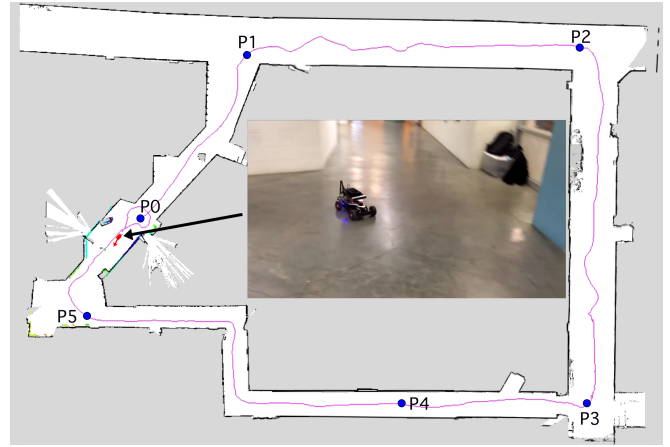


Fig. 12. Localization trail for a two minute sample of manually driving the RACECAR around the stata basement loop. Positions marked in blue correspond to markers on Figure 13. Small red arrow shows car's end position, corresponding to the image overlaid in the map. The map shown is a version of the Basement map modified for real-world accuracy.

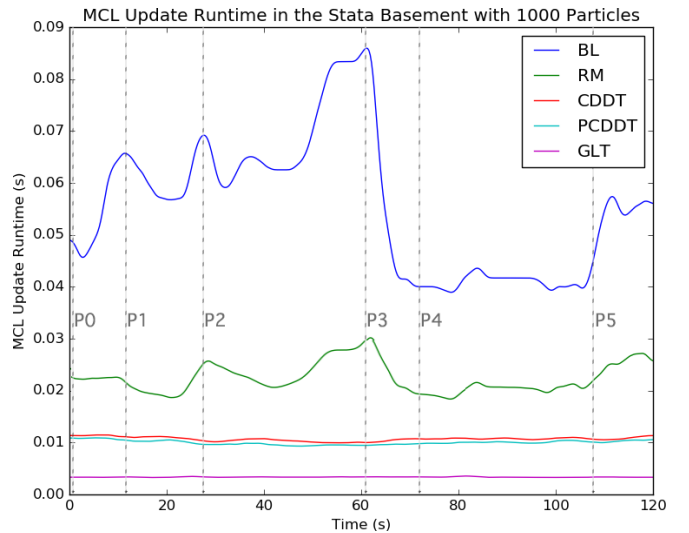


Fig. 13. Time required by the MCL update step of the particle filter algorithm with different ray casting methods over a two minute trial on the RACECAR. In all cases, the particle filter maintains 1000 particles, resolving 61 ray casts per particle.  $\theta_{discretization} = 120$  where applicable. Real-world position of the car at times marked P0-P5 shown in Figure 12.

Max particles maintained at 40Hz with 61 rays/particle				
BL	RM	CDDT	PCDDT	GLT
400	1000	2400	2500	8500

Fig. 14. Maximum number of particles that can be maintained in real time (approx. 40Hz) on the NVIDIA Jetson TX1. Stata basement map, 61 ray casts per particle,  $\theta_{discretization} = 120$  where applicable.

Our sensor model is designed for the Hokuyo UST-10LX lidar scanner used aboard the RACECAR platform, which features a 270° field of view. Since this FOV is in excess of 180°, we exploit radial symmetry discussed in the subsection IV-C to simultaneously ray cast in the  $\theta$  and  $\theta + \pi$  direction when possible. This optimization reduces the number of data structure traversals required by a third, while still resolving the same number of ray casts. As is standard in such

applications, we down-sample the laser scanner resolution to reduce the number of ray casts per sensor model evaluation, and to make the probability distribution over the state space less peaked.

During particle filter execution, we track the amount of time the Monte Carlo update step takes, including the particle resampling, motion model, and sensor model steps. Figure 13 demonstrates the MCL execution time over a two minute dataset collected on the RACECAR while driving around the Stata basement loop. We find that the BL and RM cause in significant variance in sensor model resolution time, depending on the location of the car, and the nearby map geometry. Specifically, BL and RM tend to be fast in constrained environments such as narrow hallways where beams are short on average, and slow in wide open area where beams are long on average (Fig. 12, 13). In contrast, with the CDDT or GLT based methods, the MCL update step has very little location dependent variance in execution time. This finding is in line with our expectations given the long tail performance of BL and RM, and the theoretically near constant time nature of CDDT and GLT. In a real time setting, highly variable algorithm runtimes are problematic as one must budget for the worst-case execution time.

It is interesting to note that GLT provides very fast performance in the particle filter, roughly 3.4 times faster than PCDDT. We believe this is due to the tightly clustered memory access pattern of a well-localized particle filter, which yields a good low-level cache hit rate.

## VII. CONCLUSIONS

This work demonstrates that the proposed CDDT algorithm may be used in mobile robotics to accelerate sensor model computation when localizing in a two dimensional occupancy grid map. While the precomputed LUT approach is generally 1.1 to 3.4 times faster than the proposed algorithm, the memory footprint of the proposed data structure

is approximately two orders of magnitude smaller, which may be desirable for resource constrained systems. Other than the LUT approach, CDDT is significantly faster than the other methods evaluated. Ray marching is the next best, ranging from 1.28 to 2.4 times slower than PCDDT depending on access patterns and environmental factors. The comparison with the widely used Bresenham’s Line algorithm is more stark, ranging from a factor of 6.83 to 14.8 in our benchmarks.

While our experiments reveal a multi-modal distribution of completion times for CDDT ray cast queries, it does not exhibit a significant long tail distribution, confirming our constant time analysis. We suspect the various modes in completion time are due to short circuit cases in our implementation, as well as caching effects.

In future work we aim to further develop our approach to allow for incremental map updates without requiring a full reconstruction of the underlying acceleration data structure, a feature which currently only the slowest evaluated method supports. Additionally, we plan to implement the CDDT algorithm in CUDA C++ for parallelized execution on graphics processing hardware.

## REFERENCES

- [1] J. Bresenham. “Algorithm for Computer Control of a Digital Plotter,” *IBM Systems Journal*, vol. 4, no. 1, pp. 25-30, 1965.
- [2] K. Perlin and E. M. Hoffert. “Hypertexture,” *Computer Graphics*, vol. 23, no. 3, pp. 297-306, 1989.
- [3] D. Fox, W. Burgard, and S. Thrun. “Markov localization for mobile robots in dynamic environments,” *Journal of Artificial Intelligence Research*, vol. 11, pp. 391-427, 1999.
- [4] M. Pharr, and R. Fernando. “Chapter 8. Per-Pixel Displacement Mapping with Distance Functions” in *GPU gems 2: Programming techniques for high-performance graphics and general-purpose computation*, 3rd ed. United States: Addison-Wesley Educational Publishers, 2005.
- [5] K. Zuiderveld, A. Koning, and M. Viergever. “Acceleration of ray-casting using 3D distance transforms,” *Proceedings of the SPIE*, vol. 1808, pp. 324-335, 1992.